RESEARCH ACTIVITIES IX
Center for Integrative Bioscience

IX-A Molecular Mechanisms of Oxygen Activation by Heme Enzymes

By sharing a common prosthetic group, the heme enzymes such as cytochrome P450s, peroxidases, and catalases catalyze their own unique biological functions; monooxygenation, hydrogen peroxide dependent oxidation, and dismutation of hydrogen peroxide, respectively. Our efforts have been focused on the elucidation of the structure-biological function relationship of these heme enzymes by employing both enzymatic systems including mutants and their model systems.

IX-A-1 Molecular Engineering of Myoglobin: The Improvement of Oxidation Activity by Replacing Phe-43 with Tryptophan

OZAKI, Shin-ichi[1]; HARA, Isao; MATSUI, Toshitaka; WATANABE, Yoshihito
([1]Yamagata Univ.)

[*Biochemistry* **40**, 1044 (2001)]

The replacement of Phe-43 in sperm whale myoglobin (Mb) by a tryptophan residue has been investigated to examine if an electron rich oxidizable amino acid residue in the heme vicinity increases oxidation activities of Mb. F43W Mb exhibits approximately 6- and 8-fold higher V_{max} values than the wild type in guaiacol and ABTS oxidations, respectively. However, the one-electron oxidation activity for F43W/H64L Mb is less that that of the F43W single mutant because the absence of histidine in the distal heme pocket suppresses the compound I formation. More than 15-fold improvement versus wild type Mb in the rates of two-electron oxidation of thioanisole and styrene are observed by the Phe-43 $\rightarrow$ Trp mutation. Our results indicate that Trp-43 in the mutants enhances both one- and two-electron oxidation activities (*i.e.* F43W Mb > Wild type Mb and F43W/H64L Mb > H64L Mb). The value of ^{18}O incorporation from $H_2{}^{18}O_2$ into the epoxide product for the wild type is 31%; however, the values for F43W and F43W/H64L Mb are 75 and 73%, respectively. Thus, Trp-43 in the mutants does not appear to be utilized as protein radical site in the oxidation. Furthermore, compound I of F43W/H64L Mb exhibits an absorption spectrum typical for a ferryl porphyrin radical cation, which is reduced back to the ferric state at the rate of 360 s^{-1} in the presence of thioanisole. The rate is approximately 10-fold greater than the value for H64L Mb. Our results suggest that a tryptophan in the active site of Mb mutants increases the reactivity of compound I, but the enhanced reactivity is not associated with a stable protein radical formation in the heme pocket. The oxidative protein modification of F43W/H64L Mb observed during the reaction with *m*-chlorobenzoic acid (*m*CPBA) has also been reported.

IX-A-2 Oxidative Modification of Tryptophan-43 in the Heme Vicinity of the F43W/H64L Myoglobin Mutant

HARA, Isao; UENO, Takafumi; OZAKI, Shin-ichi[1]; ITOH, Shinobu[2]; LEE, Ken-ichi[3]; UEYAMA, Norikazu[3]; WATANABE, Yoshihito
([1]Yamagata Univ.; [2]Osaka City Univ.; [3]Osaka Univ.)

[*J. Biol. Chem.* **276**, 36067 (2001)]

The F43W/H64L Mb mutant was previously constructed to investigate the effects of electron-rich tryptophan residue in the heme vicinity on the catalysis, (Figure 1) and we found that Trp-43 in the mutant was oxidatively modified in the reaction with *m*-chloroperbenzoic acid (*m*CPBA). To identify the exact structure of the modified tryptophan in this study, the *m*CPBA-treated F43W/H64L mutant has been digested stepwise with Lys-C achromobacter and trypsin, and two oxidation products are isolated by preparative FPLC. The close examinations of the ^1H NMR spectra of peptide fragments reveal that two forms of the modified tryptophan must have 2,6-disubstituted indole substructures. The ^{13}C NMR analysis suggests that one of the modified tryptophan bears a unique hydroxyl group at the amino-terminal. The results together with Ms/Ms analysis (30 Da increase in mass of Trp-43) indicate that oxidation products of Trp-43 are 2,6-dihydro-2,6-dioxoindole and 2,6-dihydro-2-imino-6-oxoindole derivatives. (Figure 2) Our finding is the first example of the oxidation of aromatic carbons by the myoglobin mutant system.

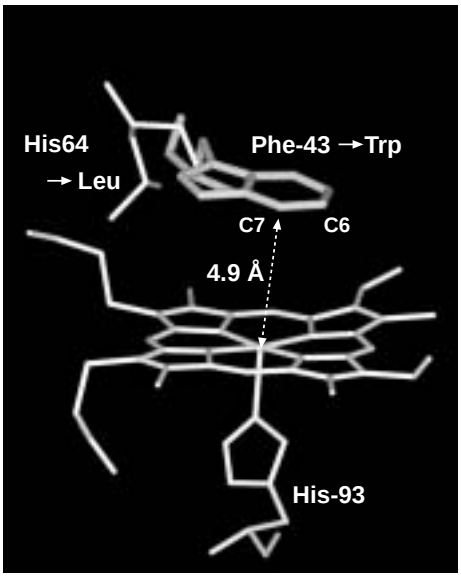

Figure 1. Calculated structure of F43W/H64L Mb using the Insight II molecular modeling program (Biosym MSI, San Diego, CA).

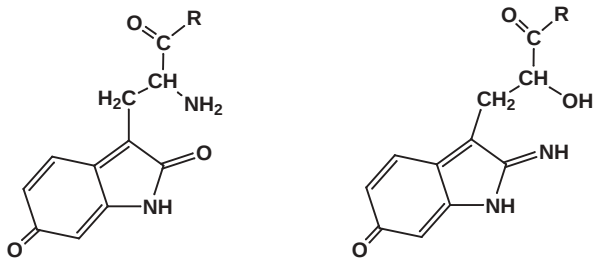

Figure 2. The oxidation products of Trp-43; (a) 2,6-dihydro-2,6-dioxoindole and (b) 2,6-dihydro-2-imino-6-oxoindole derivatives.

IX-B Model Studies of Non-Heme Proteins

Non-heme proteins play important roles in biological redox processes. Many reactions catalyzed by the non-heme enzymes are quite similar to those by hemoproteins. We are interested in the active intermediates responsible for oxidation and oxygenation by non-heme enzyme, especially the similarity and differences.

IX-B-1 (Catecholato)iron(III) Complexes: Structural and Functional Models for the Catechol-bound Iron(III) Form of Catechol Dioxygenases

YAMAHARA, Ryo[1]; OGO, Seiji; MASUDA, Hideki[1]; WATANABE, Yoshihito
([1]Nagoya Inst. Tech. and IMS)

[*J. Inorg. Biochem.* in press]

The metabolic conversion of aromatic compounds to aliphatic compounds is of fundamental importance in biology. Catechol dioxygenases are mononuclear non-heme iron enzymes that catalyze the oxygenation of catechols to aliphatic acids via the cleavage of aromatic rings. These enzymes can be divided into two types: intradiol-cleaving enzymes which break the catechol C1–C2 bond, and extradiol-cleaving enzymes which break the C2–C3 or C1–C6 bond. In the last 20 years, a number of (catecholato)iron(III) complexes have been synthesized and characterized as structural and functional models for the catechol-bound iron(III) form of catechol dioxygenases. This review collects the structural and spectroscopic characteristics and oxygenation activity of (catecholato)iron(III) complexes as structural and functional models for the catechol-bound iron(III) form of catechol dioxygenases.

IX-B-2 Biomimetic Intradiol-Cleavage of Catechols with Incorporation of Both Atoms of O_2: The Role of the Vacant Coordination Site on the Iron Center

OGO, Seiji; YAMAHARA, Ryo[1]; FUNABIKI, Takuzo[2]; MASUDA, Hideki[1]; WATANABE, Yoshihito
([1]Nagoya Inst. Tech. and IMS; [2]Kyoto Univ.)

[*Chem. Lett.* in press]

Since Hayaishi *et al.* have revealed that an intradiol-cleaving catechol dioxygenase, pyrocatechase, catalyzes the oxygenation of catechol to muconic acid with incorporation of two oxygen atoms of O_2 (but not of H_2O), the oxygenation mechanisms of catechol dioxygenases have been studied through investigations of model systems as well as the enzymes themselves. However, details of the O_2 insertion and aromatic ring-cleavage reactions are not yet understood. Herein, we report the first example of model system to display intradiol-cleavage of catechols with incorporation of two oxygen atoms of O_2 promoted by iron complexes (Figure 1): $[Fe^{III}(^3L)(DBC)(DMF)]$ {**1**, ^3L = *N*-(2-hydroxyphenyl)-*N*-(2-pyridylmethyl)benzylamine, DBC = 3,5-di-*tert*-butylcatecholato, DMF = *N*,*N*-dimethylformamide} and $[Fe^{III}(^3L)(DBC)Cl](PPh_4)$ (**2**).

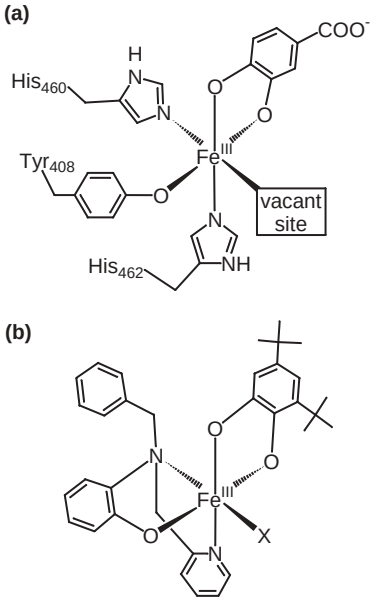

Figure 1. (a) Active site structure of a protocatechuic acid-bound form of protocatechuate 3,4-dioxygenase and (b) complexes **1** (X = Cl) and **2** (X = DMF).

IX-C Aqueous Organometallic Chemistry

Development of water-soluble organometallic catalysts is a worthy endeavor because of potential advantages such as reaction-specific pH selectivity, introduction of new biphasic processes, and alleviation of environmental problems associated with the use of organic solvents. Although the majority of these studies have been carried out with water-soluble organometallic complexes containing water-soluble phosphine ligands, few have utilized organometallic complexes containing water molecules as ligands (*i.e.* organometallic aqua complexes). These organometallic aqua complexes are promising new pH-selective catalysts since their structures drastically change as a function of pH due to deprotonation of the H_2O ligands.

IX-C-1 pH-Dependent Transfer Hydrogenation, Reductive Amination, and Dehalogenation of Water-Soluble Carbonyl Compounds and Alkyl Halides Promoted by Cp*Ir Complexes

OGO, Seiji; MAKIHARA, Nobuyuki; KANEKO, Yuichi[1]; WATANABE, Yoshihito
([1]Kochi Univ.)

[*Organometallics* in press]

Recently, we reported a pH-dependent transfer hydrogenation of water-soluble carbonyl compounds with an aqua complex $[Cp^*Ir^{III}(H_2O)_3]^{2+}$ (**1**, Cp* = η^5-pentamethylcyclopentadienyl) as a catalyst precursor and HCOONa as a hydrogen donor. We have extended our study with **1** to that with $[(Cp^{\wedge}py)Ir^{III}(H_2O)_2]^{2+}$ {**2**, Cp^py = η^5-(tetramethylcyclopentadienyl)-methylpyridine} and $[Cp^*Ir^{III}(bpy)(H_2O)]^{2+}$ (**3**, bpy = 2,2'-bipyridine), since we expect that the ligation of pyridine and bipyridine in **1** could change its catalytic activity due to the change of the Lewis acidity of the iridium ion. Herein, we report preliminary findings of pH-dependent transfer hydrogenation, reductive amination, and dehalogenation of water-soluble carbonyl compounds and alkyl halides with **1**, **2**, and **3** as catalyst precursors and HCOONa and $HCOONH_4$ as hydrogen donors. The pH-dependence in these reactions is discussed on the basis of (i) deprotonation processes of the catalyst precursors, (ii) pH-dependent behavior of the hydrogen donors, and (iii) pH-dependent formation of the active catalysts.

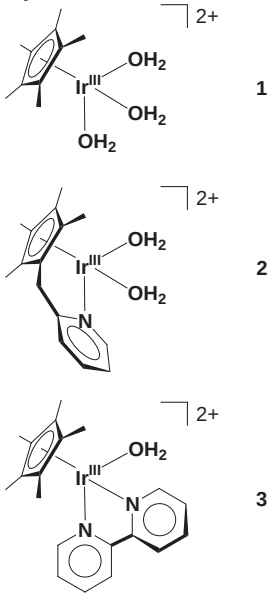

Figure 1. Complexes **1**, **2**, and **3**.

IX-D Single-Molecule Physiology

A single molecule of protein (or RNA) enzyme acts as a machine which carries out a unique function in cellular activities. To elucidate the mechanisms of various molecular machines, we need to observe closely the behavior of individual molecules, because these machines, unlike man-made machines, operate stochastically and thus cannot be synchronized with each other. By attaching a tag that is huge compared to the size of a molecular machine, or a small tag such as a single fluorophore, we have been able to image the individual behaviors in real time under an optical microscope. Stepping rotation of the central subunit in a single molecule of F_1-ATPase has been videotaped, and now we can discuss its detailed mechanism. RNA polymerase has been shown to be a helical motor that rotates DNA during transcription. Single-molecule physiology is an emerging field of science in which one closely watches individual, 'live' protein/RNA machines at work and examines their responses to external perturbations such as pulling and twisting. I personally believe that molecular machines operate by changing their conformations. Thus, detection of the conformational changes during function is our prime goal. Complementary use of huge and small tags is our major strategy towards this end.

IX-D-1 Resolution of Distinct Rotational Substeps by Submillisecond Kinetic Analysis of F_1-ATPase

YASUDA, Ryohei[1,2]; NOJI, Hiroyuki[1]; YOSHIDA, Masasuke[1,3]; KINOSITA, Kazuhiko, Jr.[1,2]; ITOH, Hiroyasu[1,4]
([1]CREST Team 13; [2]Keio Univ.; [3]Tokyo Inst. Tech.; [4]Hamamatsu Photonics)

[*Nature* **410**, 898 (2001)]

The enzyme F_1-ATPase has been shown to be a rotary motor in which the central γ-subunit rotates inside the cylinder made of $\alpha_3\beta_3$ subunits. At low ATP concentrations, the motor rotates in discrete 120° steps, consistent with sequential ATP hydrolysis on the three β-subunits. The mechanism of stepping is unknown. Here we show by high-speed imaging that the 120° step consists of roughly 90° and 30° substeps, each taking only a fraction of a millisecond. ATP binding drives the 90° substep, and the 30° substep is probably driven by release of a hydrolysis product. The two substeps are separated by two reactions of about 1 ms, which together occupy most of the ATP hydrolysis cycle. This scheme probably applies to rotation at full speed (~130 revolutions per second at saturating ATP) down to occasional stepping at nanomolar ATP concentrations, and supports the binding-change model for ATP synthesis by reverse rotation of F_1-ATPase.

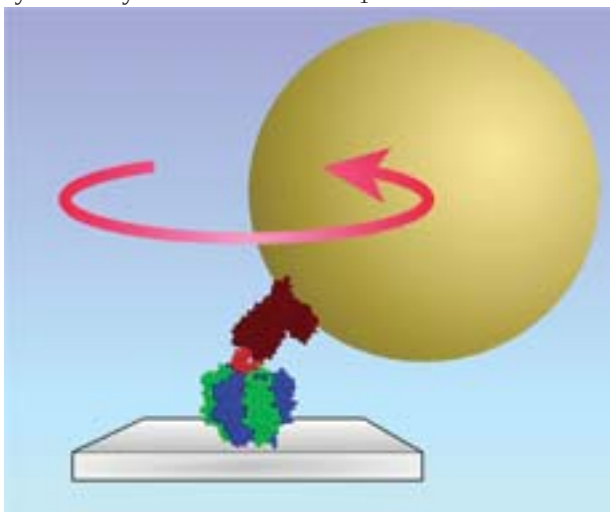

Figure 1. Imaging F_1 rotation through a gold bead. The cylinder made of three α (blue) and three β (green) subunits was fixed on a glass surface, and a 40-nm gold bead was attached to the central γ subunit (red) through streptavidin and BSA (brown) that served as glue. When the bead was attached obliquely as shown in the figure, rotation of the γ subunit resulted in a circular movement of the bead image. The rotation angle was estimated from the circular trajectory of the bead movement.

IX-D-2 Purine but Not Pyrimidine Nucleotides Support Rotation of F_1-ATPase

NOJI, Hiroyuki[1,2]; BALD, Dirk[1,3]; YASUDA, Ryohei[1]; ITOH, Hiroyasu[1,4]; YOSHIDA, Masasuke[1,3]; KINOSITA, Kazuhiko, Jr.[1,5]
([1]CREST Team 13; [2]PREST; [3]Tokyo Inst. Tech.; [4]Hamamatsu Photonics; [5]Keio Univ.)

[*J. Biol. Chem.* **276**, 25480 (2001)]

The binding change model for the F_1-ATPase predicts that its rotation is intimately correlated with the changes in the affinities of the three catalytic sites for nucleotides. If so, subtle differences in the nucleotide structure may have pronounced effects on rotation. Here we show by single-molecule imaging that purine nucleotides ATP, GTP, and ITP support rotation but pyrimidine nucleotides UTP and CTP do not, suggesting that the extra ring in purine is indispensable for proper operation of this molecular motor. Although the three purine nucleotides were bound to the enzyme at different rates, all showed similar rotational characteristics: counterclockwise rotation, 120° steps each driven by hydrolysis of one nucleotide molecule, occasional back steps, rotary torque of ~40 piconewtons (pN)·nm, and mechanical work done in a step of ~80 pN·nm. These latter characteristics are likely to be determined by the rotational mechanism built in the protein structure, which purine nucleotides can energize. With ATP and GTP, rotation was observed even when the free energy of hydrolysis was –80 pN·nm/molecule, indicating ~100% efficiency. Reconstituted F_oF_1-ATPase actively translocated protons by hydrolyzing ATP, GTP, and ITP, but CTP and UTP were not even hydrolyzed. Isolated F_1 very slowly hydrolyzed UTP (but not CTP), suggesting possible uncoupling from

rotation.

IX-D-3 Direct Observation of DNA Rotation during Transcription by *Escherichia coli* RNA Polymerase

HARADA, Yoshie[1,2]; OHARA, Osamu[3]; TAKATSUKI, Akira[1]; ITOH, Hiroyasu[2,4]; SHIMAMOTO, Nobuo[5]; KINOSITA, Kazuhiko, Jr.[1,2]
([1]Keio Univ.; [2]CREST Team 13; [3]Kazusa DNA Res. Inst.; [4]Hamamatsu Photonics; [5]Natl. Inst. Genetics)

[*Nature* **409**, 113 (2001)]

Helical filaments driven by linear molecular motors are anticipated to rotate around their axis, but rotation consistent with the helical pitch has not been observed. 14S dynein and non-claret disjunctional protein (ncd) rotated a microtubule more efficiently than expected for its helical pitch, and myosin rotated an actin filament only poorly. For DNA-based motors such as RNA polymerase, transcription-induced supercoiling of DNA supports the general picture of tracking along the DNA helix. Here we report direct and real-time optical microscopy measurements of rotation rate that are consistent with high fidelity tracking. Single RNA polymerase molecules attached to a glass surface rotated DNA for .100 revolutions around the right-handed screw axis of the double helix with a rotary torque of > 5 pN nm. This real-time observation of rotation opens the possibility of resolving individual transcription steps.

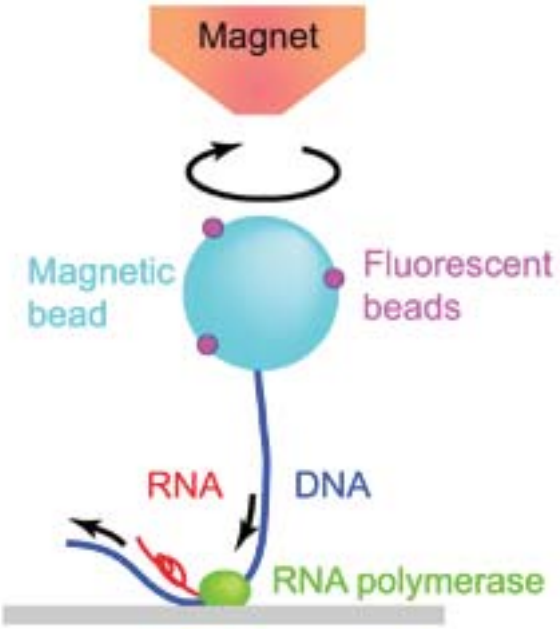

Figure 1. Observation of DNA rotation by RNA polymerase. The magnetic bead was pulled upwards by a disk-shaped neodymium magnet, to which a conical iron piece was attached to enhance the magnetic force. Magnetization was vertical and did not prevent bead rotation. Daughter fluorescent beads served as markers of rotation.

IX-E Electronic Structure and Reactivity of Active Sites of Metalloproteins

Metalloproteins are a class of biologically important macromolecules that have various functions such as oxygen transport, electron transfer, oxidation, and oxygenation. These diverse functions of metalloproteins have been thought to depend on the ligands from amino acid, coordination structures, and protein structures in immediate vicinity of metal ions. In this project, we are studying the relationship between the structures of the metal active sites and functions of metalloproteins.

IX-E-1 Structural Model of Active Site of Protocatechuate 3,4-Dioxygenase: Trigonal Bipyramidal Ferric Aqua Complex with Sterically Hindered New Salen Ligand

FUJII, Hiroshi

Protocatechurate 3,4-dioxygenase (3,4-PCD) has been found in soil bacteria and known to serve as a part of degrading aromatic molecules in nature. The enzyme is classified into an intradiol dioxygenase and contains a ferric iron as a catalytic reaction site. The enzyme cleaves catechol analogies bound to ferric iron site into aliphatic products with incorporating both atoms of molecular. It has been proposed that the enzyme activates an iron bound catecholate to react with an oxygen molecule, but not an iron bound oxygen molecule as most non-heme iron enzymes. Thus, the structure of the ferric iron site has been thought essential to understand the unique reaction of 3,4-PCD. Previous crystal structure of 3,4-PCD from *Pseudomonas putida* reveals a unique trigonal bipyramidal ferric iron site with four endogenous protein ligands (Tyr408, Tyr447, His460, and His462) and a solvent-derived water molecule. To understand the structure-function relationship of 3,4-PCD, there have been attempted over several decades to prepare inorganic model complexes that mimic the ferric iron site of 3,4-PCD, however, no ferric iron complex with the same coordination structure that in the enzyme has been characterized definitively. In this paper, we report the successful attainment to the ferric iron active site of 3,4-PCD by using sterically hindered salen ligand (Figure 1). Characterization of the present model complex reveals the roles of the iron bound water ligand in the enzyme on the unique trigonal bipyramidal structure and the catechol degradation reaction.

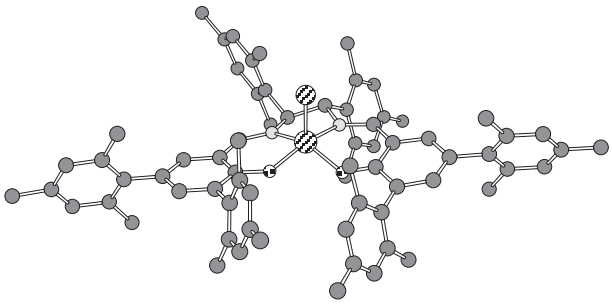

Figure 1. Structure of sterically hindered iron(III) salen complex prepared in this project.

IX-E-2 Synthesis and Characterization of High Valent Iron Porphyrin Complexes as Models for Reaction Intermediates of Cytochrome *c* Oxidase

FUJII, Hiroshi; FUMOTO, Yumiko[1]; ONO, Noboru[1]
([1]Ehime Univ.)

Cytochrome c oxidase (CcO) is the terminal oxidase that reduces molecular oxygen to water, coupling with proton pumping across the mitochondrial inner membrane. Since discovery of this enzyme, many structural and functional studies have been done to understand its reaction mechanism. Recent X-ray analyses reveal that this enzyme contains a binuclear center, heme-a_3-Cu_B site, as a reaction site. The binuclear center of the resting enzyme is ferric/cupric form. The binuclear active site is reduced to a ferrous/cuprous form by two electrons from cytochrome c through the Cu_A and heme a site. The ferrous/cuprous form of active site reacts with O_2 to yield an internal dioxygen adduct, intermediate A state, which is further converted to intermediate P and F by the aid of the electrons and protons. Although the intermediates P and F have been studied by resonance Raman and flash-flow absorption spectroscopies, the electronic states of these intermediates are not still clear. To reveal the electronic states of these intermediates and to understand the reaction mechanism of CcO, we have synthesized model complexes of the heme-a_3 site of cytochrome c oxidase. The model complex contains a formyl group at pyrrole-β position to mimic the heme a_3 and mesityl groups to stabilize high valent oxo iron species (see Figure 1). We have succeeded in the preparation of a high valent oxo iron porphyrin complex as a model for the intermediate P by the oxidation of the ferric model complex with mCPBA or ozone.

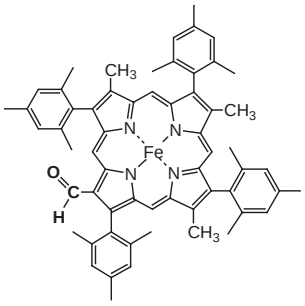

Figure 1. Structure of model complex prepared in this project as models for heme-a and heme-a_3 site of cytochrome c oxidase.

IX-F Molecular Mechanism of Heme Degradation and Oxygen Activation by Heme Oxygenase

Heme oxygenase (HO), an amphipathic microsomal proteins, catalyzes the regiospecific oxidative degradation of iron protoporphyrinIX (heme) to biliverdinIXα, carbon monoxide, and iron in the presence of NADPH-cytochrome P-450 reductase, which functions as an electron donor. Heme oxygenase reaction is the biosynthesis processes of bile pigments and CO, which is a possible physiological messenger. Recent development in the bacterial expression of a soluble form of heme oxygenase has made it possible to prepare in the large quantities for structural studies. In this project, we are studying the molecular mechanism of heme degradation and the oxygen activation by heme oxygenase using various spectroscopic methods.

IX-F-1 A Role for Highly Conserved Carboxylate, Aspartate-140, in Oxygen Activation and Heme Degradation by Heme Oxygenase-1

FUJII, Hiroshi; ZHANG, Xuhong[1]; TOMITA, Takeshi[2]; IKEDA-SAITO, Masao[2]; YOSHIDA, Tadashi[1]
([1]Yamagata Univ.; [2]Tohoku Univ.)

[*J. Am. Chem. Soc.* **123**, 6475 (2001)]

Heme oxygenase (HO) catalyzes the oxygen-dependent degradation of heme to biliverdinIXα, CO, and free iron ion via three sequential monooxygenase reactions. Although the distinct active site structure of HO from cytochrome P450 families suggests unique distal protein machinery to activate molecular oxygen, the mechanism and the key amino acid for the oxygen activation have not been clear. To investigate the functionality of highly conserved polar amino acids in the distal helix of HO-1, we have prepared alanine mutants: T135A, R136A, D140A, and S142A, and found drastic changes in the heme degradation reactions of D140A. In this paper, we report the first evidence that D140 is involved in the oxygen activation mechanism in HO-1. The heme complexes of HO mutants examined in this study fold and bind heme normally. The pKa values of the iron bound water and autooxidation rates of the oxy-form are increased with R136A, D140A, and S142A mutations, but are not changed with T135A mutation. As the wild type, T135A, R136A, and S142A degrade heme to verdohemeIXα with H_2O_2 and to biliverdinIXα with the NADPH reductase system. On the other hand, D140A heme complex forms compound II with H_2O_2 and no heme degradation occurs. For the NADPH reductase system, the oxy form of D140A heme complex is accumulated in the reaction and only 50% of heme is degraded. The stopped flow experiments suggest that D140A can not activate iron bound dioxygen and hydroperoxide properly. To investigate the carboxylate functionality of D140, we further replaced D140 with glutamic acid (D140E), phenylalanine (D140F), and asparagine (D140N). D140E degrades heme normally but D140N shows reactivity similar to D140A. D140F loses heme degradation activity completely. All of these results indicate that the carboxylate at position 140 is essential to activate the iron bound dioxygen and hydroperoxide. On the basis of the present findings, we propose an oxygen activation mechanism involving the hydrogen-bonding network through the bridging water and D140 side chain.

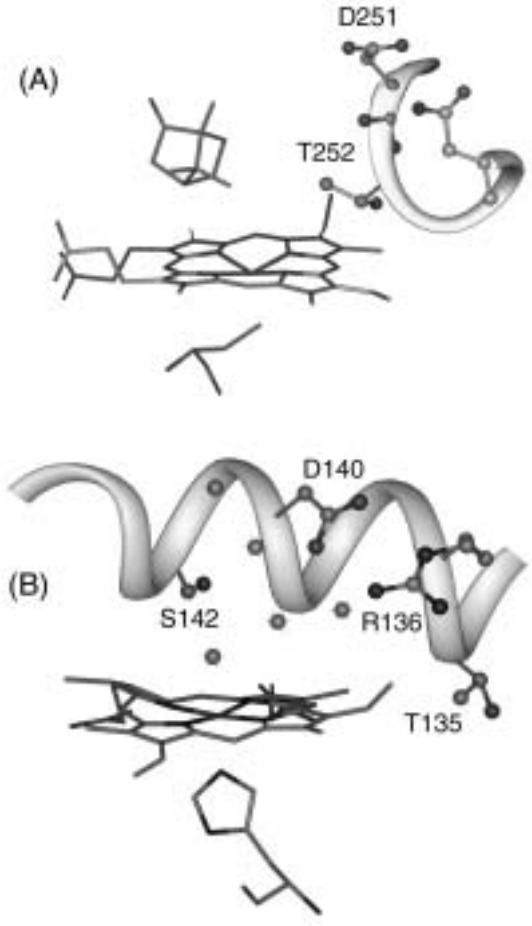

Figure 1. Active site structures of cytochrome P450 (A) and heme oxygenase (B).

IX-F-2 Catalytic Mechanism of Heme Oxygenase Through EPR and ENDOR of Cryoreduced Oxy-Heme Oxygenase and Asp 140 Mutants

DAVYDOV, Roman[1]; KOFMAN, Viktoria[1]; FUJII, Hiroshi; YOSHIDA, Tadashi[2]; IKEDA-SAITO, Masao[3]; HOFFMAN, M. Brian[1]
([1]Uni. Northwestern; [2]Yamagata Univ.; [3]Tohoku Univ.)

[*J. Am. Chem. Soc.* in press]

Heme oxygenase (HO) catalyzes the O_2- and NADPH-cytochrome P450 reductase-dependent conversion of heme to biliverdin and CO through a process in which the heme participates both as prosthetic group and substrate. It was proposed that the first mono-oxygenation step of HO catalysis is the conversion of the heme to α-meso-hydroxyheme, through a process in which an electron provided by NADPH-cytochrome P450 reductase reduces the first heme to the ferrous state and molecular of dioxygen binds to form a metastable O_2-bound complex, which then is reduced by a second electron to generate hydroperoxy ferric-HO. It was further thought that the hydroperoxy-ferric HO is the reactive hydroxylating species, rather than a high-valent ferryl active intermediate as in the case of cytochrome P450cam. However, neither the putative hydroperoxo-ferric-HO intermediate nor the a-meso-hydroxyheme product had been detected during physiological HO catalysis until our recent EPR and ENDOR study of oxy-ferrous HO cryoreduced at 77 K. In the present study we have generated a detailed reaction cycles for the first mono-oxygenation step of HO catalysis. We employed EPR and ^{1}H, ^{14}N ENDOR spectroscopies to characterize the intermediates generated by 77 K radiolytic cryoreduction and subsequent annealing of wild-type oxy-HO and D140A, F mutants.

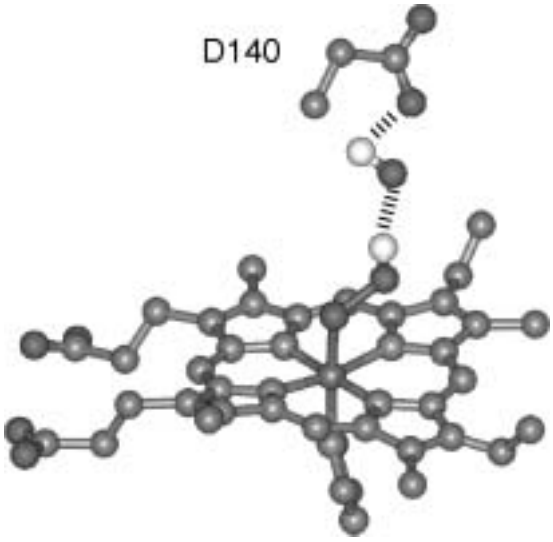

Figure 1. Structure of ferric hydroperoxide intermediate in HO.

IX-G Biomolecular Science

Elucidation of a structure-function relationship of metalloproteins is a current subject of this group. The primary technique used for this project is the stationary and time-resolved resonance Raman spectroscopy excited by visible and UV lasers. The main themes that we want to explore are (1) mechanism of oxygen activation by enzymes, (2) mechanism of active proton translocation and its coupling with electron transfer, (3) coupling mechanism of proton- and electron transfers by quinones in photosynthetic reaction center, (4) higher order protein structures and their dynamics, and (5) reactions of biological NO. In category (1), we have examined a variety of terminal oxidases, cytochrome P450s, and peroxidases, and also treated their enzymatic reaction intermediates by using the mixed flow transient Raman apparatus and the Raman/absorption simultaneous measurement device. For (2) the third generation UV resonance Raman (UVRR) spectrometer was constructed and we are going to apply it to a giant protein like cytochrme c oxidase. More recently, we succeeded in pursuing protein folding of apomyoglobin by combining UV time-resolved Raman and rapid mixing device. In (3) we succeeded in observing RR spectra of quinones A and B in bacterial photosynthetic reaction centers for the first time, but we have focused our attention on detecting tyrosine radical for the P intermediate of terminal oxidases. Some positive evidence was obtained for cytochrome bo. For (4) we developed a novel technique for UV resonance Raman measurements based on the combination of the first/second order dispersions of gratings and applied it successfully to 235-nm excited RR spectra of several proteins including mutant hemoglobins and myoglobins. Nowadays we can carry out time-resolved UVRR experiments with nanosecond resolution to discuss protein dynamics. With the newly developed third generation UV Raman spectrometer, we have succeeded in isolating the spectrum of tyrosinate in ferric Hb M Iwate, which was protonated in the ferrous state, and the deprotonated state of Tyr244 of bovine cytochrome c oxidase. As a model of Tyr244, an imidazole-bound *para*-cresol was synthesized and its UV resonance Raman was investigated. For (5) we purified soluble guanylate cyclase from bovine lung and observed its RR spectra. To further investigate it, we are developing an expression system of this protein.

IX-G-1 Presence of the Heme-oxo Intermediate in Oxygenation of Carbon Monoxide by Cytochrome c Oxidase Revealed by Resonance Raman Spectroscopy

KIM, Younkyoo[1]; SHINZAWA-ITOH, Kyoko[2]; YOSHIKAWA, Shinya[2]; KITAGAWA, Teizo
([1]Hankuk Univ.; [2]Himeji Inst. Tech.)

[*J. Am. Chem. Soc.* **123**, 757 (2001)]

Resonance Raman and absorption spectra were examined for the species generated upon incubation of oxidized bovine cytochrome c oxidase at pH 8.0 with carbon monoxide in the presence or absence of O_2. The anaerobic incubation yielded the CO isotope sensitive bands at 517 and 578 cm^{-1} for $^{12}C^{16}O$, at 512 and 563 cm^{-1} for $^{13}C^{16}O$, at 508 and 574 cm^{-1} for $^{12}C^{18}O$, and at 503 and 557 cm^{-1} for $^{13}C^{18}O$, indicating the formation of heme $a_3{}^{2+}CO$ adduct. The aerobic incubation with CO employing both $^{16}O_2$ and $^{18}O_2$ yielded the oxygen isotope-sensitive bands at 804 and 768 cm^{-1}, respectively. These bands were identified by excitation at 441.6 and 607 nm but not at 413.1, 421.3, and 590 nm, a result which is consistent with the P intermediate absorption maxima occurring near 439 and 607 nm. The frequencies of the oxygen isotope sensitive bands are in agreement with those observed for the P intermediate in the O_2 reduction by the fully reduced enzyme and in the H_2O_2 reduction by the oxidized enzyme. The other ironoxo species, the F intermediate, observed for both of the above referenced reactions was not generated in this study.

IX-G-2 Protein Conformation Change of Myoglobin upon Ligand Binding Probed by Ultraviolet Resonance Raman Spectroscopy

HARUTA, Nami[1]; AKI, Michihiko[2]; OZAKI, Shin-ichi[3]; WATANABE, Yoshihito; KITAGAWA, Teizo
([1]GUAS; [2]Univ. Tokyo; [3]Yamagata Univ.)

[*Biochemistry* **40**, 6956 (2001)]

Conformational change of myoglobin (Mb) accompanied by binding of a ligand was investigated with the 244 nm-excited ultraviolet resonance Raman spectroscopy (UVRR). The UVRR spectra of native sperm whale (sw) and horse (h) Mbs and W7F and W14F swMb mutants for the deoxy and CO-bound states enabled us to reveal the UVRR spectra of Trp7, Trp14, and Tyr151 residues, separately. The difference spectra between the deoxy and CO-bound states reflected the environmental or structural changes of Trp and Tyr residues upon CO binding. W3 band of Trp7 near the N-terminus exhibited a change upon CO binding, while Trp14 did not. Tyr151 in the C-terminus also exhibited a definite change upon CO binding, but Tyr103 and Tyr146 did not. The spectral change of Tyr residues was characterized through solvent effects of a model compound. The corresponding spectral differences between CO- and *n*-butylisocyanide-bound forms were much smaller than those between the deoxy and CO-bound forms, suggesting that the conformation change in the C- and N- terminal regions is induced by the proximal side of heme through the movement of iron. Although the swinging up of His64 upon binding of a bulky ligand is noted by X-ray crystallographic analysis, UVRR spectra of His for *n*-butylisocyanide bound form did not detect the exposure of His64 to solvent.

IX-G-3 UV Resonance Raman Characterization of Model Compounds of Tyr^{244} of Bovine Cytochrome *c* Oxidase in Its Neutral-, Deprotonated Anion-, and Deprotonated Neutral Radical-Forms: Effects of Covalent Binding between Tyrosine and Histidine

AKI, Michihiko[1]; NARUTA, Yoshinori[2]; LE, T. Huu[2]; SATO, Teizi[2]; KITAGAWA, Teizo
([1]Univ. Tokyo; [2]Kyushu Univ.)

[*J. Phys. Chem.* in press]

A model compound of Tyr^{244}-His^{240} of bovine cytochrome c oxidase was synthesized and examined with UV resonance Raman (UVRR) as well as UV visible absorption spectroscopy and pH titration. Owing to the covalent linkage between imidazole and phenol, the pKa of phenolic OH and imidazolic $N_\delta H$ groups were lowered by 1.1 and 2.3, respectively. UVRR measurements of *ortho*-imidazole-bound *para*-cresol (Im♦CrOH), its deprotonated anion (Im♦CrO^-), and deprotonated neutral radical (Im♦$CrO^\bullet$), and their imidazole perdeuterated, cresol perdeuterated, and ^{18}O derivatives allowed assignments of Raman bands to the imidazole and phenol modes. Unexpectedly, some of imidazole vibrations were resonance enhanced upon $\pi\pi^*$ transition of phenol, although they were not observed for the corresponding equimolar mixture of imidazole and *p*-cresol, indicating delocalization of π electrons between the imidazole and phenol rings via the covalent linkage. Such features were appreciably changed by incorporation of a bulky group at imidazole C^2 position, causing staggered conformation. The C–O stretching RR band was observed only for a radical state at 1530 cm^{-1}. Y8a band is not shifted upon deprotonation, although it was shifted by 12 cm^{-1} for unmodified *p*-cresol. The UVRR difference spectra of the anion and radical with regard to the neutral states are discussed in relation with the corresponding difference spectra of the enzyme.

IX-G-4 Synthesis, Structure, and H_2O_2-Dependent Catalytic Functions of Disulfide-Bridged Dicopper(I) and Related Thioether-Copper(I) and Thioether-Copper(II) Complexes

OHTA, Takehiro; TACHIYAMA, Takashi[1]; YOSHIZAWA, Kazunari[1]; YAMABE, Tokio[1]; UCHIDA, Takeshi; KITAGAWA, Teizo
([1]Kyoto Univ.)

[*Inorg. Chem.* **39**, 4358 (2000)]

A disulfide-bridged dicopper(I) complex, $[Cu_2(Py_2SSPy_2)](ClO_4)_2$ (**1**) (Py_2SSPy_2 = bis{2-[*N*,*N*-bis(2-pyridylethyl)amino]-1,1-dimethylethyl}disulfide), a thioether-copper(I) complex, $[Cu(^iPrSPy_2)](ClO_4)$ (**2**) ($^iPrSPy_2$ = *N*-(2-isopropylthio-2-methyl)propyl-*N*,*N*-bis-2-(2-pyridyl)ethylamine), and a thioether-copper(II) complex, $[Cu(PheSPy_2)(H_2O)](ClO_4)_2$ (**3**) ($PheSPy_2$ = *N*-(2-methyl-2-phenethylthio)propyl-*N*,*N*-bis-2-(2-pyridyl)ethylamine), were newly synthesized by the reactions of $Cu(ClO_4)_2\cdot 6H_2O$ with a thiol ligand of Py_2-SH (*N*,*N*-bis[2-(2-pyridyl)ethyl]-1,1-dimethyl-2-mercaptoethylamine) and thioether ligands of $^iPrSPy_2$ and $PheSPy_2$, respectively. For complexes **1** and **2**, X-ray analyses were performed. Complex **1** crystallizes in the triclinic space group $P\bar{1}$, and complex **2** crystallizes in the orthorhombic space group *Pbca* with the following unit cell parameters: for **1**, a = 15.165 (3) Å, b = 22.185 (4) Å, c = 14.989 (3) Å, α = 105.76 (1)°, β = 90.82 (2)°, γ = 75.23 (1)°, and Z = 2; for **2**, a = 17.78 (2) Å, b = 17.70 (1) Å, c = 15.75 (1) Å, and Z = 8. Complex **1** is the first structurally characterized example obtained by the redox reaction Cu(II) + RSH → Cu(I) + RSSR and has two independent structures (**1a**, **1b**) which mainly differ in S–S bond distances, Cu(I)···Cu(I) separations, and C–S–S–C dihedral angles of the disulfide units. The S–S bond distances of 2.088(7) Å in **1a** and 2.070(7) Å in **1b** are indicative of significant activation of the S–S bonds by the dicopper centers. Fragment molecular orbital (FMO) analyses and molecular orbital overlap population (MOOP) analyses based on the extended Hükel method clarify the preferable formation of the disulfide S–S bond in **1** rather than the formation of a thiolate-copper(II) complex within the Py_2S^- ligand framework. Catalytic functions of complexes **1**–**3** were investigated with peroxides (H_2O_2 and ^{t}BuOOH) as oxidants. Complex **1** catalyzed the selective oxidation of cyclohexane to cyclohexanol and mediated the cyclohexene epoxidation in the presence of H_2O_2. A transient dark green intermediate observed in the reaction of **1** with H_2O_2 is characterized by UV-vis, EPR, and resonance Raman spectroscopies, identifying it as a Cu(II)–OOH species, **1**(OOH). The resonance Raman features of the ν(O–O) bands at 822 and 836 cm^{-1}, which are red-shifted to 781 and 791 cm^{-1}, respectively, upon introduction of $H_2{}^{18}O_2$, are indicative of formation of two kinds of Cu–OOH species rather than the Fermi doublet and the significant weakening of the O–O bonds. These mechanistic studies demonstrate that by virtue of the electron-donating ability of the disulfide unit the Cu–OOH species can be actually activated for one-electron oxidation, which has been reported so far unfavorable for other vibrationally characterized Cu–OOH species.

IX-G-5 UV Resonance Raman Detection of a Ligand Vibration on Ferric Nitrosyl Heme Proteins

TOMITA, Takeshi[1]; HARUTA, Nami[2]; AKI, Michihiko[3]; KITAGAWA, Teizo; IKEDA-SAITO, Masao[1]
([1]Tohoku Univ.; [2]GUAS; [3]Univ. Tokyo)

[*J. Am. Chem. Soc.* **123**, 2666 (2001)]

The Fe^{3+}–nitric oxide (NO) complexes formed from the reactions of NO with heme proteins are of significant physiological relevance. Microbial denitrification catalyzed by cytochrome P450nor, is initiated by the formation of a Fe^{3+}–NO complex. The delivery of NO by a blood-sucking insect, *Rhodnius prolixus*, to its victims is via the ferric, not ferrous, NO complex of nitrophorin. The affinity of NO for Fe^{3+} is

much lower than that for Fe^{2+}, thereby facilitating the transfer of NO. While vibrational spectroscopy has been applied extensively to explore heme-ligand systems, its application to Fe^{3+} heme-NO complexes have been scarce, primarily because of the weak vibrational signals from the NO moieties. Thus, the development of an efficient and highly sensitive method to detect the ligand vibrations in Fe^{3+} heme NO complexes is necessary. Here, we report an innovative and highly sensitive UV resonance Raman (RR) spectroscopic method for detecting the NO stretching frequency of a variety of Fe^{3+} NO heme proteins, including myoglobin (Mb), horseradish peroxidase (HRP), mammalian heme oxygenase isoform 2 (HO-2), and FixLH.

IX-G-6 Elucidation of the Differences between the 430 and 455-nm Absorbing Forms of P450-Isocyanide Adducts by Resonance Raman Spectroscopy

TOMITA, Takeshi[1]; OGO, Seiji; EGAWA, Tsuyoshi[2]; SHIMADA, Hideo[2]; OKAMOTO, Noriaki[3]; IMAI, Yoshio[3]; WATANABE, Yoshihito; ISHIMURA, Yuzuru[2]; KITAGAWA, Teizo
([1]Tohoku Univ.; [2]Keio Univ.; [3]Osaka Prefecture Univ.)

[*J. Biol. Chem.* **276**, 36261 (2001)]

Alkylisocyanide adducts of microsomal P450 exist in two interconvertible forms, each giving the Soret maximum around 430 or 455 nm. This is demonstrated with a rabbit liver P4502B4. Resonance Raman spectra of the 430 and 455 nm forms were examined with typical P450s of the two types as well as with P450 2B4, because the 430 nm form of P4502B4 is liable to change into P420. P450cam and P450nor were selected as a model of the 430 and 455 nm forms, respectively. For *n*-butyl isocyanide (CNBu) adduct, the Fe(II)–CNBu stretching band was observed for the first time at 480/467 cm^{-1} for P450cam and at 471/459 cm^{-1} for P450nor with their ^{12}CNBu/^{13}CNBu derivatives. For P450cam, another ^{13}C-isotope sensitive bands were observed at 412/402, 844/835, and 940/926 cm^{-1}, but not with P450nor. The C–N stretching mode was identified by FTIR at 2116/2080 cm^{-1} for P450cam and at 2148/2108 cm^{-1} for P450nor for the ^{12}C/^{13}C derivatives. These findings suggest that the binding geometry of isocyanide differs between the two forms, bent and linear structures for P450camCNBu and P450norCNBu, respectively. In contrast, in the ferric state, the Raman ^{13}C isotopic frequency shifts and the IR C–N stretching frequencies (2213/2170 and 2215/2172 cm^{-1}) were similar between P450cam and P450nor, suggesting similar bent structures for both.

IX-G-7 Observation of an Isotope Sensitive Low Frequency Raman Band Specific to Metmyoglobin

HIROTA, Shun[1]; MIZOGUCHI, Yasutaka[1]; YAMAUCHI, Osamu[2]; KITAGAWA, Teizo
([1]Nagoya Univ.; [2]Kansai Univ.)

[*J. Biol. Inorg. Chem.* in press]

An iron(III)-histidine stretching (ν_{Fe-His}) Raman band is searched through isotope-sensitivity for low frequency resonance Raman bands of *metMb*, *metHb*, and its α and β subunits. A band at 218 cm^{-1} of natural abundance *metMb* exhibited a low frequency shift for ^{15}N-His-labeled *metMb* (–1.4 cm^{-1} shift), while the strong porphyrin bands at 248 and 271 cm^{-1} did not shift significantly. The frequency of the 218-cm^{-1} band of *metMb* decreased by 1.6 cm^{-1} in D_2O, probably due to N_δ-deuteration of the proximal His, in a similar manner to that of the ν_{Fe-His} band of deoxyMb in the D_2O. This 218-cm^{-1} band was shifted slightly to a lower frequency in $H_2{}^{18}O$, whereas it did little upon ^{54}Fe isotopic substitution (< 0.3 cm^{-1}) presumably because of the six-coordinate structure. This band was absent for the hydroxy*metMb* and cyano*metMb*. For *metHb* and its α and β subunits, however, the frequencies of the band around 220 cm^{-1} were not D_2O-sensitive. These results suggest an assignment of the band around 220 cm^{-1} to a pyrrole tilting mode, which contains the Fe–His stretching character for *metMb* but not for *metHb* and its subunits. The differences in the isotope-sensitivity of this band in different proteins are considered to reflect the heme structure including the Fe–His geometry specific to individual proteins.

IX-G-8 A Novel Diiron Complex as a Functional Model for Hemerythrin

ARII, Hidekazu[1]; NAGATOMO, Shigenori; KITAGAWA, Teizo; MIWA, Tomohiro[1]; JITSUKAWA, Koichiro; EINAGA, Hisahiko[1]; MASUDA, Hideki[1]
([1]Nagoya Inst. Tech.)

[*J. Inorg. Biochem.* **82**, 153 (2000)]

Diiron(II) complexes with a novel dinucleating polypyridine ligand, *N*,*N*,*N*',*N*'-tetrakis(6-pivalamido-2-pyridylmethyl)-1,3-diaminopropan-2-ol (HTPPDO), were synthesized as functional models of hemerythrin. Structural characterization of the complexes, $[Fe^{II}_2$(Htppdo)(PhCOQ)$](ClO_4)_3$ (**1**), $[Fe^{II}_2$(Htppdo)((*p*-Cl)-PhCOO)$](ClO_4)_3$, (**2**), $[Fe^{II}_2$(Htppdo)((*p*-Cl)PhCOO)]-$(BF_4)_3$ (**2'**) and $[Fe^{II}_2$(tppdo)((*p*-Cl)PhCOO)$](ClO_4)_2$ (**3**), were accomplished by electronic absorption, and IR spectroscopic, electrochemical, and X-ray diffraction methods. The crystal structures of **1** and **2'** revealed that the two iron atoms are asymmetrically coordinated with HTPPDO and bridging benzoate. One of the iron centers (Fe(**1**)) has a seven-coordinate capped octahedral geometry comprised of an N_3O_4 donor set which includes the propanol oxygen of HTPPDO. The other iron center (Fe(**2**)) forms an octahedron with an N_3O_4 donor set and one vacant site. The two iron atoms are bridged by benzoate (**1**) or *p*-chlorobenzoate (**2**). On the other hand, both Fe atoms of complex **3** are both symmetrically coordinated with N_3O_4 donors and two bridging ligands; benzoate and the propanolate of TPPDO. Reactions of these complexes with dioxygen were followed by electronic absorption, resonance Raman and ESR spectroscopies. Reversible dioxygen-binding was demonstrated by observation of an intense LMCT band for O_2^{2-} to Fe(III) at 610 (**1**) and 606 nm

(**2**) upon exposure of dioxygen to acetone solutions of **1** and **2** prepared under an anaerobic conditions at –50 degreesC. The resonance Raman spectra of the dioxygen adduct of **1** exhibited two peaks assignable to the ν(O–O) stretching mode at 873 and 887 cm^{-1}, which shifted to 825 and 839 cm^{-1} upon binding of $O^{18}{}_2$. ESR spectra of all dioxygen adducts were silent. These findings suggest that dioxygen coordinates to the diiron atoms as a peroxo anion in a μ-1,2 mode. Complex **3** exhibited irreversible dioxygen binding. These results indicate that the reversible binding of dioxygen is governed by the hydrophobicity of the dioxygen-binding environment rather than the iron redox potentials.

IX-G-9 Effects of Metal Ions on the Electronic, Redox, and Catalytic Properties of Cofactor TTQ of Quinoprotein Amine Dehydrogenases

ITOH, Shinobu[1]; TANIGUCHI, Masato[2]; TAKADA, Naoki[2]; NAGATOMO, Shigenori; KITAGAWA, Teizo; FUKUZUMI, Shunichi[2]
([1]Osaka City Univ.; [2]Osaka Univ.)

[*J. Am. Chem. Soc.* **122**, 12087 (2000)]

Model compounds of novel organic cofactor TTQ (tryptophan tryptophylquinone) of quinoprotein methylamine and aromatic amine dehydrogenases have been shown to interact with a series of metal ions in anhydrous organic media. Spectroscopic analyses including UV-vis, NMR. and resonance Raman indicate that the metal ion binds to the TTQ model compounds at their *o*-quinone moiety, the binding mode of which is similar to that proposed for the interaction between cofactor TTQ and a cationic species in the native enzymes. The binding constants K_{ML} for the metal ion complexes of TTQ model compounds have been determined from the spectral changes in UV-vis due to the complex formation. Remarkable enhancement of the oxidizing ability of the TTQ model compounds by the complexation with metal ions has been demonstrated as a large positive shift in the one-electron reduction potentials E^0_{red} of the complexes as compared to those of the TTQ model compounds in metal free form (*e.g.* ΔE^0_{red} = 1.17 V for the Mg^{2+} complex and ΔE^0_{red} = 1.16 V for the Sc^{3+} complex). The complexes can oxidize not only benzylamine but also aliphatic amines in anhydrous acetonitrile, whereas no reaction takes place in the absence of the metal ion under otherwise the same experimental conditions. Kinetic studies have revealed that the reaction proceeds via a transamination mechanism involving iminoquinone and product imine intermediates to yield the oxidized products and the reduced TTQ. The ESR spectra of the half-reduced species of TTQ model compounds; *i.e.* semiquinone radical anions, are detected successfully. The spin distribution derived from the hyperfine structures indicates that the spin is partially delocalized on the indole ring connected at the 4-position of the quinone skeleton. This indicates that the indole group plays an important role as a part of the electron transfer pathway from the reduced TTQ to a blue copper protein in biological systems.

IX-G-10 Active Site Models for Galactose Oxidase Containing Two Different Phenol Groups

TAKI, Masayasu[1]; KUMEI, Hideyuki[1]; NAGATOMO, Shigenori; KITAGAWA, Teizo; ITOH, Shinobu[2]; FUKUZUMI, Shunichi[1]
([1]Osaka Univ.; [2]Osaka City Univ.)

[*Inorg. Chim. Acta* **300**, 622 (2000)]

Model complexes of the active site of galactose oxidase (GAO) have been developed using a new ligand carrying two different phenol groups, N-[(2-hydroxy-3-methylthio-5-tert-butylphenyl)methyl]-N-[(2-hydroxy-3,5-di-tert-butylphenyl)methyl]-2-(2-pyridyl)ethylamine ($L1H_2$). Deprotonated ligand $L1^{2-}$ forms a dimeric Cu(II) complex, $[Cu(II)_2(L1^{2-})_2]$, in the solid state, the structure of which has been determined by X-ray crystallographic analysis. The dimeric Cu(II)-diphenolate complex can be converted into the monomeric complex, $[Cu(II)(L1^{2-})(X)]$ (X = py, AcO, and $PhCH_2OH$), in solution by adding exogenous ligands such as pyridine (py), acetate (AcO^-), or benzyl alcohol ($PhCH_2OH$). The structure and physicochemical properties (UV-Vis, ESR, redox potential) of $[Cu(II)(L1^{2-})(X)]$ have been explored as a model for the resting state of the enzyme. One-electron oxidation of $[Cu(II)(L1^{2-})(py)]$ and $[Zn(II)(L1^{2-})(py)]$ by $(NH_4)_2[Ce^{IV}(NO_3)_6]$ (CAN) yielded the corresponding phenoxyl radical/phenolate complexes, $Cu(II)(L1^{\bullet-})$ and $Zn(II)(L1^{\bullet-})$, respectively, which have also been characterized by UV-Vis, resonance Raman, and ESR. The structure, physicochemical properties and reactivities of the diphenolate and phenoxyl radical/phenolate complexes of $L1H_2$ are compared to those of the corresponding monophenolate and monophenoxyl radical complexes in order to obtain further insight into the role of Tyr 495 in the native enzyme.

IX-G-11 Active Site Structure of SoxB-Type Cytochrome *bo*$_3$ Oxidase from Thermophilic Bacillus

UCHIDA, Takeshi; TSUBAKI, Motonari[1]; KUROKAWA, Tatsuki[2]; HORI, Hiroshi[3]; SAKAMOTO, Junshi[3]; KITAGAWA, Teizo; SONE, Nobuhito[2]
([1]Himeji Inst. Tech.; [2]Kyushu Inst. Tech.; [3]Osaka Univ.)

[*J. Inorg. Biochem.* **82**, 65 (2001)]

Two-subunit SoxB-type cytochrome *c* oxidase in *Bacillus stearothermophilus* was over-produced, purified, and examined for its active site structures by electron paramagnetic resonance (EPR) and resonance Raman (RR) spectroscopies. This is cytochrome bo_3 oxidase containing heme B at the low-spin heme site and heme O at the high-spin heme site of the binuclear center. EPR spectra of the enzyme in the oxidized form indicated that structures of the high-spin heme O and the low-spin heme B were similar to those of SoxM-type oxidases based on the signals at g = 6.1, and g = 3.04. However, the EPR signals from the Cu_A center

and the integer spin system at the binuclear center showed slight differences. RR spectra of the oxidized form showed that heme O was in a 6-coordinated high-spin (ν_3 = 1472 cm^{-1}), and heme B was in a 6-coordinated low-spin (ν_3 = 1500 cm^{-1}) state. The Fe^{2+}–His stretching mode was observed at 211 cm^{-1}, indicating that the Fe^{2+}–His bond strength is not so much different from those of SoxM-type oxidases. On the contrary, both the Fe^{2+}–CO stretching and Fe^{2+}–C–O bending modes differed distinctly from those of SoxM-type enzymes, suggesting some differences in the coordination geometry and the protein structure in the proximity of bound CO in cytochrome *bo*$_3$ from those of SoxM-type enzymes.

IX-G-12 First Synthetic NO-Heme-Thiolate Complex Relevant to Nitric Oxide Synthase and Cytochrome P450nor

SUZUKI, Noriyuki[1]; HIGUCHI, Tsunehiko[1]; URANO, Yasuteru[1]; KIKUCHI, Kazuya[1]; UCHIDA, Takeshi; MUKAI, Masahiro[2]; KITAGAWA, Teizo; NAGANO, Tetsuo[1]
([1]Univ. Tokyo; [2]RIKEN)

[*J. Am. Chem. Soc.* **122**, 12059 (2001)]

We have already succeeded in the synthesis of a stable Fe^{III}-porphyrin-alkanethiolate complex, in which the sulfur atom is sterically protected from reactive molecules such as O_2 and NO by bulky groups. We report here some, spectroscopic and electrochemical properties of the first synthetic NO–heme–thiolate complex, prepared by the use of SR.

IX-G-13 Effects of a Thiolate Axial Ligand on the $\pi \rightarrow \pi^*$ Electronic States of Oxoferryl Porphyrins: A Study of the Optical and Resonance Raman Spectra of Compounds I and II of Chloroperoxidase

EGAWA, Tsuyoshi[1]; PROSHLYAKOV, A. Denis[2]; MIKI, Hideho[3]; MAKINO, Ryu[4]; OGURA, Takashi[5]; KITAGAWA, Teizo; ISHIMURA, Yuzuru[1]
([1]Keio Univ.; [2]Michigan State Univ.; [3]Zeon Kasei Co. Ltd.; [4]Rikkyo Univ.; [5]Univ. Tokyo)

[*J. Biol. Inorg. Chem.* **6**, 46 (2001)]

Optical absorption and resonance Raman spectra have been investigated for enzymatic intermediates, compounds I and II, of chloroperoxidase (CPO) which contains a thiolate-ligated iron porphyrin. Compound I of CPO (CPO-I), an oxoferryl porphyrin π cation radical, gave an apparently asymmetric single-peaked Soret band at 367 nm, for which band fitting analyses revealed the presence of two transition bands around 365 and 415 nm. Compound II of CPO (CPO-II), an oxoferryl neutral porphyrin, gave a split Soret spectrum with two bands (blue and red Soret bands) at 373 and 436 nm. Thus both CPO-I and CPO-II can be categorized as hyperporphyrins. The maximum extinction coefficients (ε_b and ε_r) and energies (E_b and E_r) of the blue and red Soret bands of CPO-II were found to fall on an $\varepsilon_b/\varepsilon_r$ versus E_b–E_r correlation line derived from data reported for six- coordinate ferrous derivatives of cytochrome P450 and CPO, Corresponding data for CPO-I did not fall on the correlation line. Resonance enhancement of the Fe^{IV}=O stretching (ν_{FeO}) Raman band was found for CPO-I when Raman scattering was excited at wavelengths within both transition bands around 365 and 415 nm, while the ν_{FeO} Raman band was not identified for CPO-II at any of the excitation wavelengths examined here. These findings suggest that the thiolate axial ligand causes Soret band splitting of CPO-II through configuration interaction between the sulfur $\rightarrow$ porphyrin e_g* charge transfer and porphyrin a_{1u},$a_{2u} \rightarrow e_g$* transitions, while the FeO portion is important in determining the shape of the Soret band of CPO-I.

IX-G-14 Characterization of Imidazolate-Bridged Dinuclear and Mononuclear Hydroperoxo Complexes

OHTSU, Hideki[1]; ITOH, Shinobu[2]; NAGATOMO, Shigenori; KITAGAWA, Teizo; OGO, Seiji; WATANABE, Yoshihito; FUKUZUMI, Shunichi[1]
([1]Osaka Univ.; [2]Osaka City Univ.)

[*Inorg. Chem.* **40**, 3200 (2000)]

Dinucleating ligands having two metal-binding sites bridged by an imidazolate moiety, Hbdpi, HMe_2bdpi, and Hme_4bdpi (Hbdpi = 4,5-bis(di(2-pyridylmethyl)-aminomethyl)imidazole, HMe_2bdpi = 4,5-bis((6-methyl-2-pyridylmethyl)(2-pyridylmethyl)amino-methyl)imidazole, HMe_4bdpi = 4,5-bis(di(6-methyl-2-pyridylmethyl)aminomethyl)imidazole), have been designed and synthesized as model ligands for copper-zinc superoxide dismutase (Cu, Zn–SOD). The corresponding mononucleating ligands, $MeIm(Py)_2$, $MeIm(Me)_1$, and $MeIm(Me)_2$ ($MeIm(Py)_2$ = (1-methyl-4-imidazolylmethyl)bis(2-pyridylmethyl)amine, $MeIm(Me)_1$ = (1-methyl-4-imidazolylmethyl)(6-methyl-2-pyridylmethyl) (2-pyridylmethyl)amine, $MeIm(Me)_2$ = (1-methyl-4-imidazolylmethyl)bis(6-methyl-2-pyridylmethyl)amine), have also been synthesized for comparison. The imidazolate-bridged Cu(II)–Cu(II) homodinuclear complexes represented as $[Cu_2(bdpi)(CH_3CN)_2](ClO_4)_3 \cdot CH_3CN \cdot 3H_2O$ (**1**), $[Cu_2(Me_2bdpi)(CH_3CN)_2](ClO_4)_3$ (**2**), $[Cu_2(Me_4bdpi)(H_2O)_2](ClO_4)_3 \cdot 4H_2O$ (**3**), a Cu(II)–Zn(II) heterodinuclear complex of the type of $[CuZn(bdpi)(CH_3CN)_2](ClO_4)_3 \cdot 2CH_3CN$ (**4**), Cu(II) mononuclear complexes of $[Cu(MeIm(Py)_2)(CH_3CN)](ClO_4)_2 \cdot CH_3CN$ (**5**), $[Cu(MeIm(Me)_1)(CH_3CN)](ClO_4)_2$ (**6**), and $[Cu(MeIm(Me)_2)(CH_3CN)](ClO_4)_2$ (**7**) have been synthesized and the structures of complexes **5**–**7** determined by X-ray crystallography. The complexes **1**–**7** have a pentacoordinate structure at each metal ion with the imidazolate or 1-methylimidazole nitrogen, two pyridine nitrogens, the tertiary amine nitrogen, and a solvent (CH_3CN or H_2O) which can be readily replaced by a substrate. The reactions between complexes **1**–**7** and hydrogen peroxide (H_2O_2) in the presence of a base at –80 degreesC yield green solutions which exhibit intense bands at 360–380 nm,

consistent with the generation of hydroperoxo Cu-(II) species in all cases. The resonance Raman spectra of all hydroperoxo intermediates at –80 degreesC exhibit a strong resonance-enhanced Raman band at 834–851 cm^{-1}, which shifts to 788–803 cm^{-1} (Δv = 46 cm^{-1}) when ^{18}O-labeled H_2O_2 was used, which are assigned to the O–O stretching frequency of a hydroperoxo ion. The resonance Raman spectra of hydroperoxo adducts of complexes **2** and **6** show two Raman bands at 848 (802) and 834 (788), 851 (805), and 835 (789) cm^{-1} tin the case of $H_2{}^{18}O_2$, Δv = 46 cm^{-1}), respectively. The ESR spectra of all hydroperoxo complexes are quite dose to those of the parent Cu(II) complexes except **6**. The spectrum of **6** exhibits a mixture signal of trigonal-bipyramid and square-pyramid which is consistent with the results of resonance Raman spectrum.

IX-G-15 Oxygenation of Phenols to Catechols by a (μ-η^2:η^2-peroxo)dicopper(II) Complex. Mechanistic Insight into the Phenolase Activity of Tyrosinase

ITOH, Shinobu[1]; KUMEI, Hideyuki[2]; TAKI, Masayasu[2]; NAGATOMO, Shigenori; KITAGAWA, Teizo; FUKUZUMI, Shunichi[2]
([1]Osaka City Univ.; [2]Osaka Univ.)

Mechanistic studies on the oxygenation of phenolates to the corresponding catechols by a (μ-η^2: η^2-peroxo)dicopper(ll) comp]ex have been carried out to provide sjgnificant insight into the mechanism of pheno]ase activity of tyrosinase. Treatment of [Cu-(L^{py2Bz})]PF_6 (L^{Py2BZ} = *N*,*N*-Bis[2-(2-pyridyl)ethyl]-α,α-dideuterio-benzylamine) with molecular oxygen in acetone at –94 °C gave a (μ-η^2: η^2-peroxo)dicopper(II) complex, the formation of which has been confirmed by its characteristic UV-vis [λ_{max} = 364 and 530 nm (ε = 26400 and l500 M^{-1} cm^{-1})] and resonance Raman spectra ($\nu_{O(16)–O(16)}$) = 737 cm^{-1}, $\nu o_{O(18)–O(18)}$ = 697 cm^{-1}) as well as the ESR-silence and the observed stoichiometry of Cu:O_2 = 2:1. Addition of lithium salts of *p*-substituted phenols into the solution induces oxygenation at its *o*-position to give the corresponding catechols in good yields, but no C–C or C–O coupling dimer is produced. The reaction obeys pseudo-first-order kinetics in the presence of excess amount of substrate and shows a Mjchaelis-Menten type saturation phenomenon. The reactivity of the substrates increases as the electron-donating nature of the *p*-substituent increases. In addition, no catechol formation was observed when a bis(μ-oxo)dicopper(III) was employed instead of the ((μ-η^2:η^2-peroxo)dicopper(II) complex under the same experimental conditions. All these results suggest that the oxygenation of phenolates to catechols by the ((μ-η^2:η^2-peroxo)dicopper(II) comp]ex proceeds via *electrophilic attack* of the peroxo species to the phenolate in a binary complex between the peroxo species and the substrate.

IX-G-16 Differences in Changes of Subunit Interfacial Contacts upon Ligand Binding to the α or β Subunits of Ni–Fe Hybrid Hemoglobin Probed by UV Resonance Raman Spectroscopy

NAGATOMO, Shigenori; NAGAI, Masako[1]; SHIBAYAMA, Naoya[2]; KITAGAWA, Teizo
([1]Kanazawa Univ.; [2]Jichi Medical School)

[*Biochemistry* submitted]

To see the α1-β2 subunit contacts in the half-ligated hemoglobin A (HbA), ultraviolet resonance Raman (UVRR) spectra of Ni–Fe hybrid Hb have been examined under various solution conditions. Our previous studies demonstrated that Trpβ37, Tyrα42 and Tyrα140 are mainly responsible for UVRR spectral differences between deoxyHbA and COHbA (Nagai, M., Wajcman, H., Lahary, A., Nakatsukasa, T., Nagatomo, S., and Kitagawa, T. *Biochemistry* **38**, 1243 (1999)). The half-ligated $\alpha^{Ni}\beta^{COFe}$ and $\alpha^{COFe}\beta^{Ni}$ at pH 6.7 in the presence of IHP as well as $\alpha^{Ni}\beta^{deoxy}$ and $\alpha^{deoxy}\beta^{Ni}$ stayed in the complete T structure similar to deoxyHbA. Upon ligand binding to Fe hemes, Trp residues are changed toward the R-like contact to a similar extent in $\alpha^{Ni}\beta^{CO}$ and $\alpha^{CO}\beta^{Ni}$. The spectral changes of Tyr and Trp are not synchronous and also different between $\alpha^{Ni}\beta^{COFe}$ and $\alpha^{COFe}\beta^{Ni}$. It is not until pH 8.7 with $\alpha^{Ni}\beta^{deoxy}$ that Tyr residues change upon ligand binding in the presence of IHP, while they changed at pH 6.7 in the absence of IHP. The structural change of Tyr residues is induced by binding of CO, but not NO, to α heme, while they were induced similarly by binding of CO and NO to β-heme. Structural changes of Trp residues are induced by the CO binding to either α- or β-heme. These observations directly indicate that the phenomenon occurring at the α1-β2 interface is different between ligand binding to α- and β-hemes and that it is greatly influenced by IHP. Thus in this study, we supplement our previous study on NOHb regarding the mechanism of the change of Tyr residues.

IX-G-17 Resonance Raman Studies of the Oxygen Sensing Signal Transducer Protein HemAT from *Bacillus Subtilis*

AONO, Shigetoshi[1]; KATO, Toshiyuki[1]; MATSUKI, Mayumi[1]; NAKAJIMA, Hiroshi[1]; OHTA, Takehiro; UCHIDA, Takeshi; KITAGAWA, Teizo
([1]JAIST)

[*J. Biol. Chem.* submitted]

HemAT-Bs is a heme-containing signal transducer protein responsible for aerotaxis of *Bacillus subtilis*. The recombinant HemAT-Bs expressed in *E. coli* was purified as the oxy form in which O_2 was bound to the ferrous heme. Although the electronic absorption spectra of HemAT-Bs were similar to those of myoglobin, HemAT-Bs showed some unique characteristics in its resonance Raman spectra. O_2-bound HemAT-Bs showed the ν(Fe–O_2) band at 560 cm^{-1}, which suggests a unique hydrogen bonding to the bound O_2 *i.e.*, the hydrogen bonding between a distal amino acid residue and the proximal oxygen atom of the bound O_2. Deoxy HemAT-Bs showed the ν(Fe–His) band at 225 cm^{-1}, which indicates a relatively stronger hydrogen bonding to the proximal His and/or a less strained Fe–His bond compared with myoglobin. CO-

bound HemAT-Bs showed the ν(Fe–CO) ,and ν(C–O) bands at 494 and 1964 cm^{-1}, respectively. These results indicate that a histidine is an axial ligand of the heme in HemAT-Bs.

IX-G-18 Time-Resolved UV Resonance Raman Investigation of Protein Folding: Characterization of Kinetic and Equilibrium Intermediates of Apomyoglobin

HARUTA, Nami[1]; KITAGAWA, Teizo
([1]GUAS)

[*J. Biochemistry* submitted]

The equilibrium acid-unfolding intermediate and kinetic folding intermediates of apomyoglobin were investigated by 244 nm-excited UV resonance Raman spectroscopy combined with a new rapid mixer. The dead time for mixing in the newly constructed flow-mixer was determined to be 150 μs with UV Raman spectral changes of imidazole to imidazolium upon mixing with an acid. The pH-jump experiments of apomyoglobin (apoMb) from 2.2 to 5.6 conducted with this device demonstrated the presence of three folding intermediates. Based on the analysis of W3 and W7 bands of Trp 7 and Trp14, the first intermediate, formed before 250 μs, involved inclusion of Trp14 into an α-helix from a random coil. In the second intermediate, formed around 1 ms after the start of folding, the surroundings of both Trp7 and 14 were significantly hydrophobic, suggesting the formation of hydrophobic core. In the third intermediate appearing around 3 ms, the hydrophobicity was relaxed to the same level as that of the pH 4 equilibrium intermediate, which was investigated in detail with the stationary state technique. The change from the third intermediate to the native state takes time longer than 40 ms, while the appearance of the native spectrum after the mixing of the same solutions was confirmed separately.

IX-G-19 Raman Spectroscopy of Proteins

KITAGAWA, Teizo; HIROTA, Shun[1]
([1]Nagoya Univ.)

[*The Handbook of Vibrational Sectroscopy*, Eds., J. M. Chalmers and P. R. Griffiths, vol. 5, pp. 3426–3446, John Wiley & Sons, Ltd.; Chichester U.K. (2002)]

Infrared (IR) and Raman spectroscopy are the main methods to measure the vibrational spectrum of proteins. When a molecular vibration is accompanied by a change of dipole moment, the mode is IR active, and when the vibration is accompanied by a change of polarizability, the mode is Raman active. For a molecule with a center of symmetry, mutual exclusion occurs. Accordingly, the two methods are complementary. In the case of synthetic homopolypeptides with a specific geometry, IR and Raman active modes are often different from each other because of their symmetry properties. For general proteins, however, there is no symmetry, and therefore selection rules are not helpful for band assignments. In practice, some modes are stronger for Raman and others are stronger for IR.

The most important benefit of Raman in comparison with IR spectroscopy in observing the vibrational spectra of proteins is that the measurement of aqueous solutions is much easier with the former, because the Raman scattering from water is very weak. Since the technique can be applied to crystals as well as to solutions, it is also useful to compare structures of a protein in solution and crystalline phases. Another important characteristic of Raman spectroscopy is the possibility of resonance enhancement. When the excitation wavelength of Raman scattering approaches an absorption maximum of an electronic transition of a molecule, some of the molecular vibrations gain strong enhancement of Raman intensity. This is called the resonance Raman effect. Under resonance conditions, very dilute solutions can be used for Raman measurements under conditions when ordinary Raman bands are not seen. As a result, the spectrum becomes simpler. In such a case, as detailed information on the molecular structure can be derived from the spectrum of a biopolymer with a molecular weight of 10^5 as can be found for small molecules. By selecting an appropriate excitation wavelength, different chromophores of the same molecule can be monitored. Accordingly, for colored proteins, visible excitation of Raman scattering provides structural information on a chromophore and UV excitation selectively brings about the vibrational spectra of side chains of aromatic residues and the polypeptide skeleton.

IX-G-20 Identification of Tyrosine Residues Involved in Ligand Recognition by the Phosphatidylinositol 3-Kinase Src Homology 3 Domain: Circular Dichroism and UV Resonance Raman Studies

OKISHIO, Nobuyuki[1]; TANAKA, Toshiyuki[2]; NAGAI, Masako[1]; FUKUDA, Ryuji[1]; NAGATOMO, Shigenori; KITAGAWA, Teizo
([1]Kanazawa Univ.; [2]Univ. Tsukuba)

[*Biochemistry* in press]

Src homology 3 (SH3) domains are small non-catalytic protein modules capable of mediating protein-protein interactions . We previously demonstrated that the association of a ligand peptide RLPI (RKLPPRPSK) causes environmental and structural changes of Trp55 and some of seven Tyr residues in the phosphatidylinositol 3-kinase (PI3K) SH3 domain by circular dichroism (CD) and 235-nm excited UV resonance Raman (UVRR) spectroscopies [Okishio, N., *et al. Biopolymers* **57**, 208 (2000)]. In this work, the affected Tyr residues were identified as Tyr12, Tyr14, and Tyr73 by the, CD analysis of a series of mutants, in which every single Tyr residue was replaced by a Phe residue. Among these three residues, Tyrl4 was found to be a main contributor to the UVRR spectral change upon the RLPl binding,. Interestingly, CD and UVRR analyses revealed that RLPl associates with the Y14F and Y14H mutants in different ways. These results suggest that Tyr14 plays a crucial role in the ligand recognition, and the amino acid substitution at Tyr14 affects the mode of

PI3K SH3-ligand interaction. Our findings give an insight into how SH3 domains can produce diversity and specificity to transduce a certain signal within cells.

IX-H Fast Dynamics of Photoproducts in Solution Phases

Picosecond time-resolved resonance Raman (ps-TR^3) spectroscopy is a promising technique to investigate ultrafast structural changes of molecules. However, this technique has not been used as widely as nanosecond TR^3 spectroscopy, mainly due to the lack of light source which has suitable repetition rates of pulses and wavelength tunability. In order to obtain qualified TR^3 spectra, first we need two independently tunable light sources for pump and probe pulses. Second, the repetition rate should be higher than kiloHertz to keep a moderate average laser power without making the photon density of probe pulse too high. We succeeded in developing light sources for ps-TR^3 spectroscopy having wide tunability and kHz repetition, and applied them to study fast dynamics of photo-excited molecules. For carbonmonoxy myoglobin (MbCO), vibrational relaxation with the time constant of 1.9 ps was observed for CO-photodissociated heme. For Ni–octaethylporphyrin in benzene, differeces in rise times of population in vibrationally excited levels among various modes were observed in the anti-Stokes spectra for the first time. This technique has been applied to identify the trans ligand of CO in the CO-bound transcriptional factor, Coo A.

On the other hand, we have constructed a nanosecond temperature-jump apparatus using a water absorption in near infrared. The new apparatus based on a Nd:YAG laser was combined with a time-resolved Raman measurement system and applied successfully to explore thermal unfolding of ribonucelase A.

IX-H-1 Ultrafast Dynamics of Myoglobin Probed by Time-resolved Resonance Raman Spectroscopy

MIZUTANI, Yasuhisa; KITAGAWA, Teizo

[*Chem. Records* **1**, 258 (2001)]

Recent experimental work on the ultrafast dynamics of myoglobin carried out in this laboratory is summarized with a stress on structural and vibrational energy relaxation. Studies on the structural relaxation of myoglobin following CO photolysis revealed that the structural change of heme itself caused by CO photodissociation is completed within the instrumental response time of the time-resolved resonance Raman apparatus used (~2 ps). In contrast, changes in the intensity and frequency of the iron-histidine (Fe–His) stretching mode upon dissociation of the trans ligand were found to occur in the picosecond regime. The Fe–His band is absent for the CO-bound form, and its appearance upon photodissociation was not instantaneous in contrast with that observed in the vibrational modes of heme, suggesting appreciable time evolution of the Fe displacement from the heme plane. The band position of the Fe–His stretching mode changed with a time constant of about 100 ps, indicating that tertiary structural changes of the protein occurred in a 100-ps range. Temporal changes of the anti-Stokes Raman intensity of the ν_4 and ν_7 bands demonstrated immediate generation of vibrationally excited heme upon the photodissociation and decay of the excited populations, whose time constants are 1.1 ± 0.6 and 1.9 ± 0.6 ps, respectively. In addition, the development of the time-resolved resonance Raman apparatus and prospects in this research field are described.

IX-H-2 Time-Resolved Resonance Raman Study of the Exciplex Formed between Excited Cu-Porphyrin and DNA

KRUGLIK, G. Sergei[1]; MOJZES, Peter[2]; MIZUTANI, Yasuhisa; KITAGAWA, Teizo; TURPIN, Pierre-Yve[3]
([1]B. I. Stepanov Inst. Phys.; [2]Charles Univ.; [3]Univ. Pierre)

[*J. Phys. Chem. B* **105**, 5018 (2001)]

The photoinduced reversible process of exciplex formation and decay between the water-soluble cationic metalloporphyrin 5,10,15,20-tetrakis[4-(*N*-methyl-pyridyl)] (Cu(T4MPyP)) and calf- thymus DNA has been studied by a picosecond time-resolved resonance Raman (ps-TR^3) technique. For a detailed analysis of the exciplex properties, the following model compounds have also been investigated: double-stranded poly-nucleotides poly(dA-dT)$_2$, poly(dG-dC)$_2$, and poly(dA-dC). poly(dG-dT), single-stranded poly(dT), and the 32-mer d[(Gr)$_7$ATAT(GC)$_7$]$_2$. Additional Raman measure-ments have also been done in using cw and 20-ns laser sources. It is shown that this reversible exciplex is formed, with a yield depending on the nucleic base sequence, in less than 2 ps after photoexcitation, between photoexcited Cu(T4MPyP) and C=O groups of thymine residues in all thymine-containing sequences of nucleic acids. Such a rapid exciplex building process implies that it involves porphyrin molecules initially located, in the steady state of this interaction, at AT sites of the nucleic acids. This has two main consequences, which contradict previously reported assumptions (Strahan *et al., J. Phys. Chem.* **96**, 6450 (1992)): (i) Although the binding mode of the porphyrin actually depends on the base sequence, there is no preferential binding of Cu(T4MPyP) to the various sites of DNA,

and (ii) there is no photoinduced ultrafast porphyrin translocation from GC to AT sites of DNA. In addition, it is shown that with surrounding water molecules an exciplex can also be formed in ~1 ps, whose spectral characteristics are not distinguishable from those formed with thymine residues. However, these two exciplex species can be distinguished from each other by their relaxation kinetics: the lifetime of the exciplex formed with water lies in the 3–12 ps range, while that of the exciplex formed with nucleic acids lies in the nanosecond time domain (1–3 ns). A set of possible routes is discussed for each of the exciplex building/decay processes.

IX-H-3 Ultrafast Structural Relaxation of Myoglobin Following Photodissociation of Carbon Monoxide Probed by Time-Resolved Resonance Raman Spectroscopy

MIZUTANI, Yasuhisa; KITAGAWA, Teizo

[*J. Phys. Chem.* **105**, 10992 (2001)]

Studies on the structural relaxation of myoglobin following CO photolysis revealed that the structural change of heme itself caused by the cleavage of the Fe–CO bond is completed within the instrumental response time (~2 ps) of the time-resolved resonance Raman apparatus used. In contrast, changes in the intensity and frequency of the iron-histidine stretching [ν(Fe–His)] mode were found to occur in the pico-second regime. The ν(Fe–His) band is absent for the CO-bound form, and its appearance upon photo-dissociation was not instantaneous in contrast with the changes observed in the vibrational modes of heme, suggesting appreciable time evolution of the Fe displacement from the heme plane. Same behaviors were observed for the model compound of the heme part without protein matrix. Therefore the intensity change in ν(Fe–His) is not associated with protein relaxation following the CO photodissociation. The band position of the ν(Fe–His) mode changed with a time constant of about 100 ps, while that of the model compound without the protein matrix showed no shift. This indicates that tertiary structural changes of the protein occurred in a 100-ps range.